Nozzle Afterbody Configuration Development for the B-1 Strategic Bomber

J. C. Sargent* and J. L. Gunter*

Rockwell International Corporation, Los Angeles, Calif.

An experimental evaluation was conducted on several aft nacelle/nozzle configurations. The wind-tunnel data are presented for different nozzle shapes, variations of the nacelle fineness ratio, and different internozzle fairing configurations. These results were used in mission studies to define the aircraft configuration. A relatively short, light-weight nozzle was integrated with the nacelle to provide better mission performance than a longer, heavier design. Increasing the nacelle fineness ratio by increasing the length reduced drag, but this was offset by the increased weight. A fixed internozzle fairing incorporating the precooler air discharge from the ECS was selected over other concepts.

Nomenclature

A_8	= nozzle throat area
A_9	= nozzle exit area
A_9/A_8	= nozzle area ratio
A_{max}	= maximum cross-sectional area of nacelle
D	= aft nacelle and nozzle external drag
D_{eq}	= diameter of a circular area equal to $A_{max} - A_9$
F_G	= nozzle gross thrust
F_{Gi}	= nozzle ideal gross thrust
FS	= fuselage station
L	= distance from A_{max} to nozzle exit plane
L/D_{eq}	= nacelle fineness ratio
M_0	= freestream Mach number
P_0	= freestream static pressure
P_{t8}	= nozzle throat total pressure
P_{t8}/P_0	= nozzle pressure ratio
q	= freestream dynamic pressure
$D/q A_{max}$	= drag coefficient
$(F_G\text{-}D)/F_{Gi}$	= gross thrust-minus-drag coefficient
α	= angle of attack
β_T	= nozzle external terminal boattail angle
θ	= nozzle internal divergence angle
Λ_{LE}	= wing sweep angle

I. Introduction

THE B-1 is a long-range strategic bomber with variable-sweep wings designed for both terrain-following near Mach 1.0 and high-altitude supersonic operation. The long-range requirements made it extremely important to obtain high-performance characteristics for both subsonic and supersonic speeds. However, the problem of achieving low drag was greater at subsonic speeds, where the nozzles were closed down for dry-power operation and presented more projected boattail area.

Nozzle/afterbody development included performance and compatibility aspects of nozzle geometry, engine length, internozzle fairings, ECS discharge, wing gloves, and horizontal tail location. Performance aspects included nacelle and nozzle-installed performance, as well as power effects on the aft fuselage closure drag. Compatibility aspects included 1) potential exhaust gas impingement on, and subsequent overheating of, the aft fuselage and horizontal tail surfaces exposed to the hot exhaust plume; 2) acoustic and pressure loads on the aft fuselage and tail surfaces as a function of engine power; 3) effects of engine power variation on aircraft stability and control; and 4) the effects of the local external flowfield on the engine/nozzle flow and thrust characteristics.

An overview of the total nozzle/afterbody development for the B-1 was presented in Ref. 1. The subject paper presents a more detailed description of the configuration evolution and experimental evaluation of the nozzle fairing design. This paper concentrates more on aerodynamic and performance features than on mechanical design aspects. A description of the final nozzle/afterbody installation is presented, and the aerodynamic problems encountered during the configuration development are discussed. The various configurations evaluated are shown, together with wind-tunnel test data.

II. Nozzle/Afterbody Installation

The B-1 propulsion system consists of two nacelles mounted under the fixed portions of the variable-sweep wing, as shown in Fig. 1. Each nacelle contains two General Electric F101 afterburning turbofan engines and nozzles. These engines are close-spaced. An ECS heat exchanger is located between the engines from which the precooler airflow is ducted back to the internozzle fairing and discharged at that station. The twin-nacelle arrangement, located under the wing, was the most efficient configuration for meeting air vehicle balance requirements, as well as for providing desired propulsion system characteristics. This arrangement permitted the nacelles to be located far enough outboard of the weapons bay to prevent interference effects during weapons delivery, but not so far outboard as to constrain the design of the variable-sweep wing. The relatively short nacelles, integrated with the wing and containing close-spaced engines, were configured to minimize wetted area and projected area. The shaping of these nacelles, as well as the fore-and-aft locations, was selected to minimize wave drag at transonic and supersonic speeds.

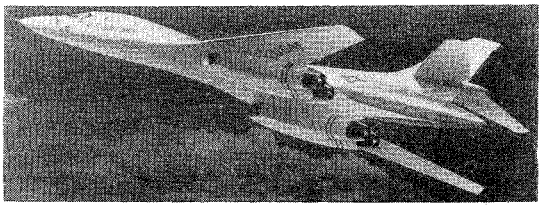

Fig. 1 Propulsion system installation on B-1.

Presented as Paper 74-1102 at the AIAA/SAE 10th Propulsion Conference, San Diego, Calif., Oct. 21-23, 1974; submitted Nov. 21, 1974; revision received April 17, 1975.

Index categories: Aircraft Aerodynamics (including Component Aerodynamics); Aircraft Performance.

*Member of the Technical Staff, B-1 Division.

The underwing location results in several airframe/exhaust system integration considerations. The wing sweep is varied over the B-1 mission, and the trailing edge of the wing moves appreciably relative to the nozzle closure, as shown in Fig. 2. Furthermore, the wing structure is flexible, with a resultant shape dependent on aircraft weight. In the aft sweep positions, wing deflection causes the trailing edge to lift up off the nacelle, shown in Fig. 2, which influences the local flowfield approaching the nozzles. Consequently, during configuration development testing, it was necessary to include both fore-and-aft wing sweeps as well as different wing deflection heights.

The ECS precooler airflow is ducted into the internozzle fairing. The internozzle fairing thus is used as a plenum. The ECS airflow then is discharged from two narrow slots adjacent to each nozzle. An isometric sketch of the arrangement is presented in Fig. 3.

A scheduled variable-area convergent-divergent (C-D) nozzle provides nozzle throat area and expansion area ratios necessary for high thrust efficiency at the key mission points. The external shape also has been integrated carefully with the nacelle shape to minimize drag. A sketch of the nozzle, showing geometries for key mission points, is presented in Fig. 4, together with pertinent geometric data.

The area ratio of this nozzle is set mechanically by the throat area to simplify the nozzle control system and save weight. The nozzle area ratio vs throat area schedule is presented in Fig. 5. As shown, low area ratios are obtained at low throat areas associated with dry-power operation at subsonic cruise points. Higher area ratios are obtained at high throat areas associated with augmented operation for the supersonic conditions, where the pressure ratios are higher and more thrust is obtained by internal expansion. However, the nozzle actuation mechanization has been designed so that the schedule can return to low area ratios at extreme throat areas associated with augmented conditions for low-speed operation such as takeoff.

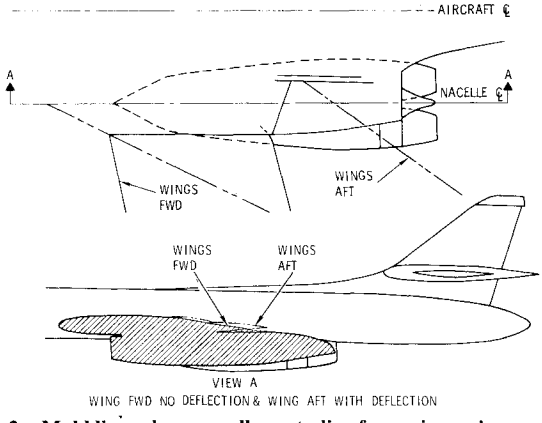

Fig. 2 Mold lines along nacelle centerline for various wing sweeps.

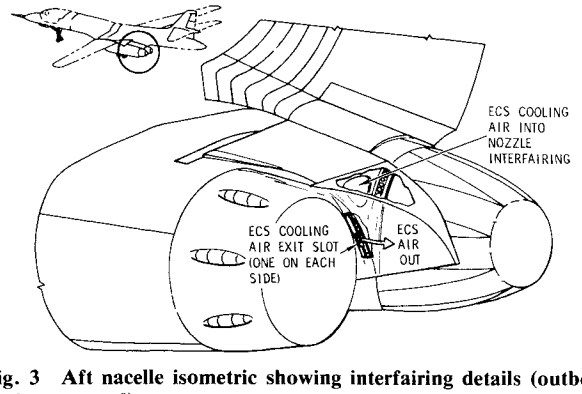

Fig. 3 Aft nacelle isometric showing interfairing details (outboard engine removed).

III. Configuration Development

Configuration development and exhaust stream/airframe compatibility testing was accomplished with a half-span subsonic development model, II, a full-span subsonic/supersonic development model, III, and a full-span hot jet model. Pressure loads data were obtained from a full-span subsonic/supersonic model. Performance verification data were obtained from an 0.06-scale full-span subsonic/supersonic model. Strut effects and inlet fairing effects also were investigated with specialized models. The test data presented in this paper were obtained from wind-tunnel tests of the B-1 nozzle/afterbody development model II. These tests were a joint effort of General Electric and Rockwell International.

Development model II is a 0.0667-scale semispan B-1 model, shown in Fig. 6. This model simulated the aircraft geometry so that effects of the rest of the airframe on nacelle/nozzle drag were accounted for. The tests were conducted in the FluiDyne Engineering Corporation's 5½ × 5½-ft transonic wind tunnel. A flow-through thrust-minus-drag

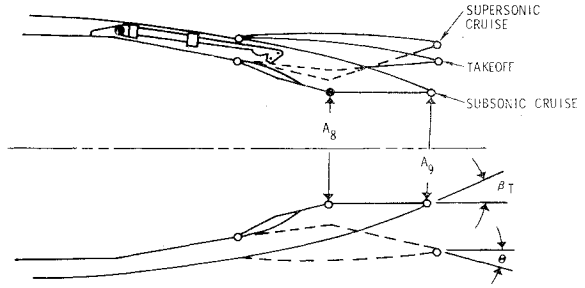

	A_9/A_8	β_T	θ
SUBSONIC CRUISE	1.03	20°	1/2°
SUPERSONIC CRUISE	1.44	10°	10°

Fig. 4 Scheduled variable-geometry nozzle for GE F101 afterburning turbofan engine.

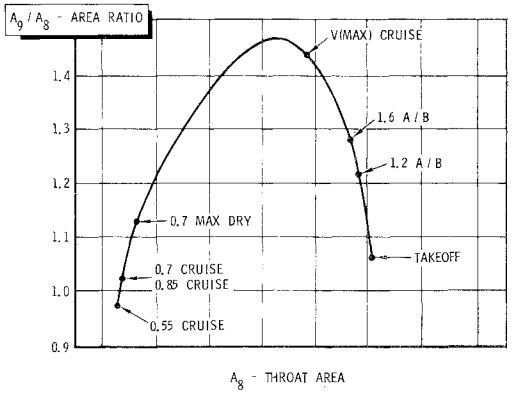

Fig. 5 Area ratio schedule for GE F101 nozzle.

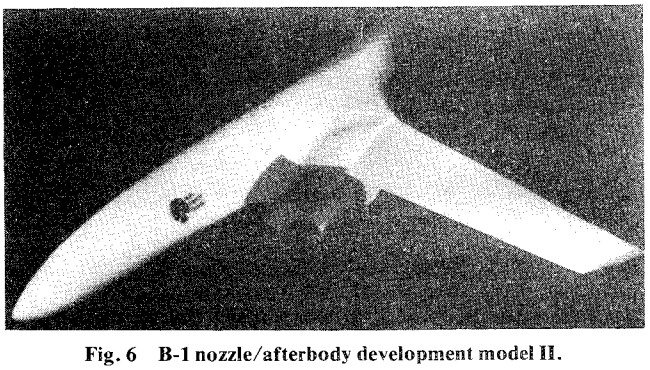

Fig. 6 B-1 nozzle/afterbody development model II.

balance was used to measure the net force of internal gross thrust less the external nozzle and nacelle drag. The metric portion of the model is shown as the shaded area in Fig. 6.

Testing provided the necessary thrust and drag data for use in mission studies to select the best of the candidate configurations. Most of the testing was at subsonic conditions. Supersonic testing, not reported herein, was carried out on an 0.036-scale full-span model (development model III). These tests also provided force and moment data on the aft fuselage and tail as a function of simulated engine power. Final performance verification testing was performed over the complete flight/power spectrum with the 0.06-scale verification model. The data from these latter tests verified the performance levels predicted from the development model tests.

Nozzle Configuration

Four nozzle design approaches were evaluated early in the configuration definition phase of the B-1 program. Each design was estimated to have slightly different thrust and weight characteristics. Actuation, cooling, and burner volume requirements for each design also dictated different external shapes. A wind-tunnel test program was conducted to determine the resultant drag of each design as integrated with the nacelle and the rest of the airframe so that total mission performance studies could be conducted, and the better design selected.

The four nozzle configurations tested are shown in Fig. 7. Configuration 1 employed long movable flaps with actuators contained within the flaps. For configuration 2, the actuators were removed from the flaps, the flaps were shortened, and the nozzle was moved aft to provide more burner volume. The actuators were located around the tailpipe forward of the nozzle hinge line. Configuration 3 employed the same nozzle as configuration 2, but the afterburner was shortened. Configuration 4 had the same overall length as configuration 3 but employed a different actuation scheme, which resulted in a slightly different external shape for the nozzle and around the actuators. A comparison of the mold lines along the top or bottom engine centerline is presented in Fig. 7.

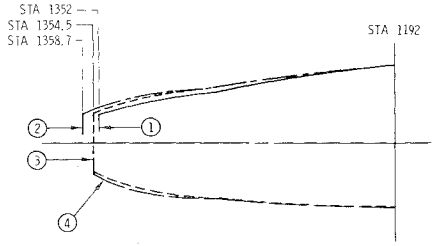

Fig. 7 Comparison of external mold lines for four nozzle/nacelle configurations tested.

Tests results are presented in Fig. 8 in terms of thrust-minus-drag of the total aft nacelle divided by ideal gross thrust of both nozzles vs nozzle pressure ratio. All four configurations were tested at Mach numbers of 0.70 and 0.85, as shown in Figs. 8a and 8b. Nozzles 2 and 4 were eliminated from further testing by preliminary screening, and nozzles 1 and 3 were tested further at Mach 0.55. The static performance ($M_0 = 0$) is also presented in Fig. 8a for reference purposes. Configuration 1 had the highest performance at all conditions tested. However, this was due primarily to higher internal performance thrust-minus-drag coefficient being about 1% higher at $M_0 = 0.0$ (Fig. 8a). Estimates of full-scale nozzle internal performance indicated that configuration 1 would have values equal or lower than the other designs due to more leakage area with the longer flaps.

Mission performance and range values were calculated for all four-nozzle candidates, using the resulting installed incremental drag values (compared to a common reference drag) from the test, and using estimated internal gross thrust values and estimated engine weights. Results showed that nozzle concept 3 was best on both subsonic and supersonic missions. Consequently, this nozzle design was selected for the B-1, and General Electric commenced the augmentor/nozzle design and development.

Nacelle Fineness Ratio

During the evolution of the B-1 configuration, the cross-sectional area of the nacelle/wing combination was increased to take advantage of the structural efficiency offered by the

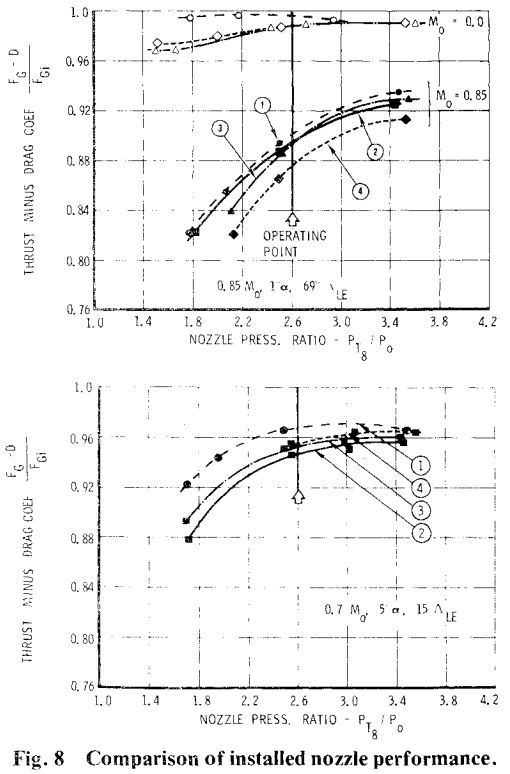

Fig. 8 Comparison of installed nozzle performance.

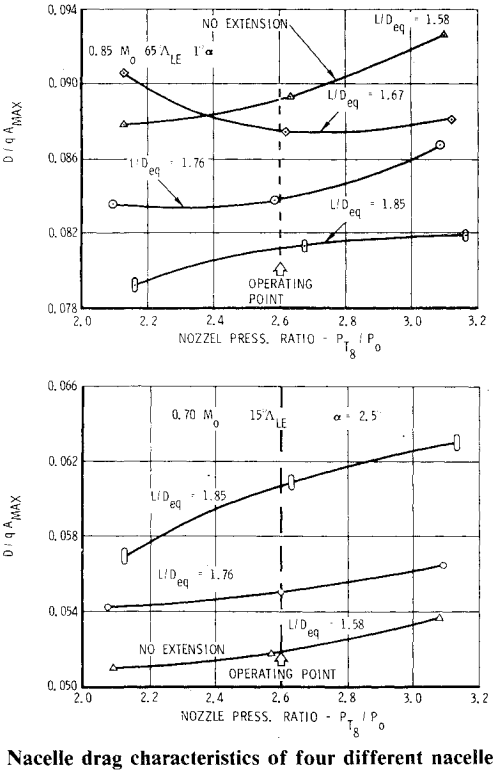

Fig. 9 Nacelle drag characteristics of four different nacelle lengths tested.

blended wing-body. Although the total aircraft performance was improved by this concept, drag on the aft nacelle and nozzles was increased due to a lower nacelle fineness ratio, L/D_{eq}. A study was conducted to explore the performance advantages of increasing the fineness ratio by lengthening the nacelle. The manner of lengthening the nacelle was to increase the engine tailpipe length (which, incidently, provided more thrust at the supersonic speeds).

Installed engine performance and engine/nacelle weight estimates were made for the following three extensions: L/D_{eq} = 1.67, 1.76, and 1.85, compared to the basic L/D_{eq} = 1.58. A wind-tunnel test program was conducted to define the subsonic drag characteristics of each extension compared to the basic configuration. The nacelle lines of the model were refaired for each extension so that the nozzle blended smoothly into the nacelle lines.

The results of the tests are presented in Fig. 9 for the 0.70 and 0.85 M_0 conditions tested. Static, internal nozzle performance was the same for all four configurations, and so the data are presented in terms of an afterbody drag coefficient, $D/q\,A_{max}$, vs nozzle pressure ratio. The drag is for the total aft nacelle, two nozzles, and interfairing. The A_{max} is the maximum cross-sectional area of the nacelle and wing which was on the balance.

As shown in Fig. 9a, at $M_0 = 0.85$, the longer engine extensions resulted in lower drag. The L/D_{eq} = 1.85 extension reduced the total aft nacelle/nozzle drag about 10% at the operating point. However, at 0.70 M_0 (Fig. 9b) with the wings well forward, the longer extensions resulted in higher drag due to increased wetted area. The increased drag at 0.70 M_0 just about equals the decreased drag at 0.85 M_0.

The variation of drag with fineness ratio at 0.85 M_0 is presented in Fig. 10, together with an estimated variation. The measured drag values do not decrease with increasing fineness ratio as rapidly as the estimate. The estimates were based on previous data wherein the fineness ratio was changed by increasing the cross-sectional area, thus increasing local boattail angles and projected area. The fineness ratio for the test data presented in Fig. 10 was varied by increasing length only. This reduces local boattail angles, but the projected area remains the same.

The incremental drags derived from the test data presented in Fig. 9 were combined with weight estimates and with internal engine/nozzle installed performance estimates, and mission studies were conducted. The results of these studies indicated that the L/D_{eq} = 1.76 extension was the most favorable of the three extensions studied. However, because of the increased weight, the air vehicle performance improvement at 0.85 M_0 was not sufficient to offset the performance loss at 0.70 M_0. The impact on range for the subsonic mission was a net loss of 6 miles and, for the supersonic mission, a gain of 7 miles. Consequently, the L/D_{eq} = 1.58 extension (basic configuration) was retained on the air vehicle.

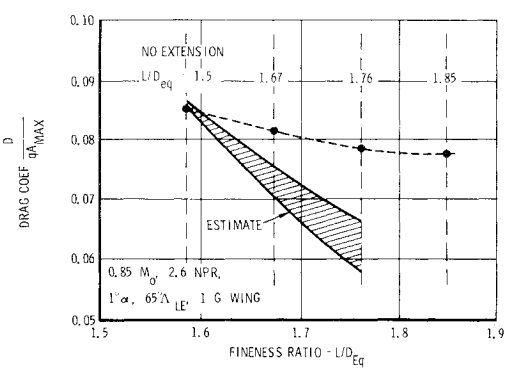

Fig. 10 Effect of fineness ratio on nacelle drag.

Internozzle Fairing Configuration

Fairing out the area between the two engines of a twin-engine nacelle has been the subject of several past programs.[2,3] Although close-spaced engines result in lower overall drag, the fairing out of this area is more difficult than for wide-spaced designs.

During the configuration definition phase of the B-1 program, a considerable effort was devoted to this problem. Many configurations and ideas were examined. Several employed a blunt base at the station of the nozzle hinge line with the option of exhausting the precooler air from the ECS system out the base. Other configurations employed mechanical schemes of extending a fairing to the nozzle exit plane but bridging between nozzles. This required a movable (telescoping or collapsing) surface to follow the nozzle contour as the nozzle external surface varied from closed-down to full-open. Again, studies were conducted both with and without the ECS airflow being discharged out of this fairing. This configuration, incidentally, resulted in an additional mechanical interface between the engine and the airframe. Still other configurations employed fixed interfairings that extended to the nozzle exit plane but did not interfere mechanically or contact the nozzles.

An extensive internozzle fairing configuration study was conducted to define the best configuration for this area. A total of 10 internozzle fairing configurations, including ECS discharge geometries, were wind-tunnel-tested to obtain drag

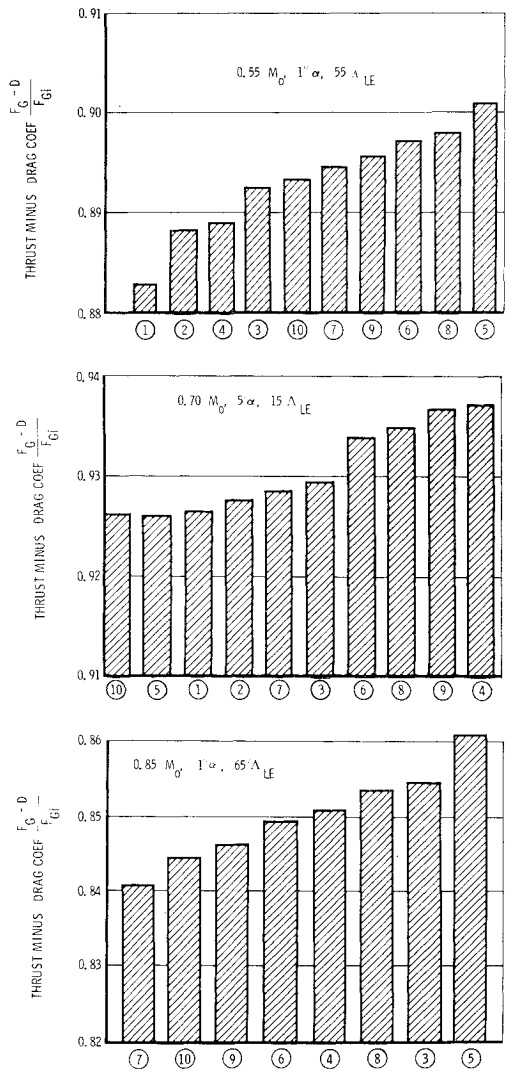

Fig. 11 Thrust-minus-drag characteristics of 10 internozzle fairing/ECS discharge configurations tested.

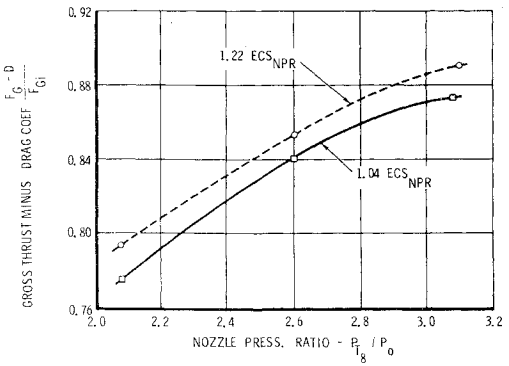

Fig. 12 Effect of ECS airflow on performance.

data. Configurations 1-4 employ a blunt base at the station of the nozzle hinge line and incorporate different geometries for exhausting the ECS precooler airflow. Configurations 5-7 and 9 employ a movable fairing (collapsing or telescoping) that follows the nozzle and has a mechanical interface between the nozzle and the airframe. The fairing for configurations 5 and 7 go only part-way along the nozzle and end in a blunt base. ECS precooler airflow is discharged at this station. Configuration 6 has no ECS precooler airflow incorporated, and it would have been necessary to discharge this airflow elsewhere. Configuration 9 was like configuration 6, except that the ECS precooler airflow was discharged out of a long, narrow slot across the top of the interfairing at the station of the nozzle hinge line. Configuration 8 was fixed interfairing (no contact with the nozzle). The ECS precooler airflow was discharged out of long slots along the side of each nozzle, as shown in Fig. 3. Configuration 10 was a blunt base at the station of the nozzle hinge line without ECS discharge.

The test results are presented in Fig. 11 in terms of the installed thrust-minus-drag coefficient of the total nacelle/nozzles at the operating pressure ratios. The momentum of the ECS airflow was not on the balance. Therefore, only the effect of this airflow on external drag was measured.

As shown, different configurations provided better performance than others at different test conditions. For instance, configuration 5 had the highest thrust-minus-drag values at 0.55 and 0.85 M_0, but configuration 4 had the highest value at 0.70 M_0. Furthermore, at the conditions where configuration 4 had the highest coefficient, configuration 5 was among the lowest, and vice versa. However, configuration 8 had one of the highest values at all three conditions tested.

The incremental drag values derived from the test data presented in Fig. 11 were combined with weight estimates for each configuration and installed engine performance and mission studies conducted. The results of the analyses indicated that configuration 8 produced from 10 to 30 miles more range than any of the other top four candidates and about 140 miles more range than configuration 10 (blunt base without ECS discharge), which was the worst. Configuration 8 had no moving parts and did not touch the nozzles and so had no mechanical interface between the engine and airframe. Configuration 8 was selected for the aircraft.

Based on this selection, a parametric wind-tunnel test was conducted to define the drag variations with the pressure ratio of the ECS airflow. This test was conducted at all conditions, and an example of this effect at 0.85 M_0 is presentd in Fig. 12. (As previously discussed, the momentum of the ECS airflow is not on the balance.) As shown in this figure, the effect of increasing the pressure ratio of the ECS airflow is to reduce drag or increase thrust-minus-drag. These data were used to describe installed engine performance as the ECS airflow is varied in flight. The data are presented here to illustrate the substantial effect that this parameter has on drag.

IV. Conclusions

This paper presents some of the highlights of the B-1 nozzle/afterbody development program. A relatively simple, light-weight configuration employing state-of-the-art technology was developed which has good performance from an overall systems and mission standpoint. The importance of evaluating concepts on an overall mission or systems basis is emphasized by the results presented in this paper, wherein final selections were made contrary to what wind-tunnel test data alone indicated. Furthermore, in most instances, a simple light-weight concept could be defined and integrated with the rest of the aircraft, which had drag levels comparable to those obtained with more idealized shapes.

During nozzle/afterbody development testing, considerable attention was given to the technique of predicting full-scale aircraft performance based on wind-tunnel test data. A straightforward answer was not found. To overcome these deficiencies in current practice, a comprehensive wind-tunnel/flight-test correlation program is needed.

References

[1] Ross, J.W., "Nozzle/Afterbody Development Program for the B-1 Strategic Aircraft," B-1 Division, Rockwell International, Los Angeles, Calif., NA-72-997, 1972.

[2] Mercer, C. E. and Berrier, R. L. "Effect of Afterbody Shape, Nozzle Type, and Engine Lateral Spacing on the Installed Performance of a Twin-Jet Afterbody Model," NASA TM X-1855, 1969.

[3] Lee, E. E. and Runkel, J. F., "Performance of Closely Spaced Twin-Jet Afterbodies with Different Inboard-Outboard Fairing and Nozzle Shapes," NASA TM X-2329, Sept. 1971.